Iranian Journal of Chemical Engineering
Vol. 3, No. 4 (Autumn), 2006, IAChE

Research note

Experimental study of the shape and motion of flattened drops in a Hele-Shaw Cell

*J. Hashemi[*1], M. Salarieh, B. Maini[2], C. R Moore[2]*

1- Petroleum University of Industry & Islamic Azad University-Ahwaz, Iran.
2- University of Calgary

Abstract

The motion and shape of a flattened drop and bubble through another continuous liquid phase (conveying phase) are investigated experimentally, using a narrow gap Hele-Shaw cell. Seven different liquid-liquid systems were tested. In all cases the continuous phase was the more viscous wetting phase. A number of observations on the shape and motion of the elongated flattened drops are noted and discussed. In the capillarity-dominated ($Ca<1.69\times10^{-6}$) region, the irregular shape of the discontinuous phase drops changed with time and position, and the drop velocity was much lower than that of the conveying phase. Three different shapes of stabilized elongated drops were observed at higher Capillary numbers. The conditions that lead to the appearance of stabilized elongated drops are discussed. The velocities of these stabilized elongated flattened drops were 2 to 4.7 times higher than that of the conveying liquid. A correlation to predict the elongated flattened drop shape as a function of the dimensionless parameters governing the system is developed based on the experimental results.

Keywords*: Drops & Bubbles, Elongated Flattened Drop, Two-phase Flow, Hele-Shaw cell, Flow in Fractures*

1. Introduction

Two-phase flow in micro-channels is of interest to researchers working in many different fields of advanced science and technology such as: micro-electro-mechanical systems, electronic cooling, chemical process engineering, bioengineering, and medical and genetic engineering. It also has applications in many other traditional fields involving multi-phase flow through fractures such as energy resource recovery (petroleum, natural gas, coal beds exploited for methane, geothermal water and steam), long-term storage of nuclear waste in deep underground repositories, which will most likely contain fractures, and movement of oleic contamination in groundwater aquifers.

Two-phase immiscible fluid flow in a fracture can occur in a number of configurations (flow patterns). Obviously the flow patterns in a fracture or Hele-Shaw cell will be different from that of macro size rectangular tubes due to the accentuated impact of surface forces. The flow structure (phase geometry and pattern) in an individual fracture and fracture network ultimately control the phases' pressure-saturation relation, permeability, solute dispersion and inter-phase mass transfer. It will also affect the flow and transport through the surrounding porous

* - Author to whom correspondence should be addressed

matrix blocks in dual porosity systems. An interesting pattern that occurs over a wide range of parameters is the slug flow, which is frequently encountered in fractured oil-wet reservoirs during the immiscible displacement of viscous oil, and in natural gas reservoirs during the displacement of water in gas production. It is characterized by the discontinuity of one phase through the second conveying phase. The slug shape can be regular in a smooth-walled fracture and is called an elongated flattened drop (or bubble). The rounded leading edge patterns may occupy a considerable portion of the fracture width and have a length of several times or several hundred times that of the cell's hydraulic diameter. However, in rough-walled fractures the slug shape may be highly irregular depending on factors such as fracture geometry and fluid properties. The analytical flow pattern necessitates the study of a single elongated flattened drop motion through a continuous liquid phase, which is as rich and complex as the viscous fingering [1]. The conditions corresponding to a swarm of the elongated flattened drops can be inferred from that of a single drop and their conglomeration. Eventually, understanding the behavior of a single fracture flow is a prerequisite to the understanding of flow in complex fracture systems.

The Hele-Shaw cell is a common simple model to study a single fracture. The non-wetting phase slug is surrounded by a thin film of continuous wetting phase on the wall sides and the bulk of the continuous phase elsewhere (Fig. 1). Capillary, gravitational, and viscous forces play an important role in determining the slug flow pattern and shape in micro-channels. In this paper the motion and shape of a flattened drop through a more viscous continuous liquid phase are investigated experimentally using a Hele-Shaw cell. A qualitative description of different flow regimes depending on the experimental conditions is reported. A correlation between the drop deformation and the dimensionless numbers of the flow conditions is also proposed.

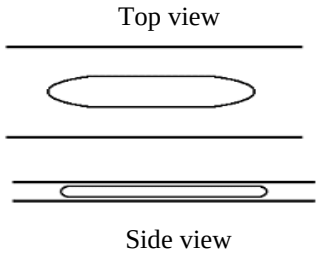

Figure 1. Slug interface typical shape schematic, in Hele-Shaw cell.

Taylor and Saffman[2] reported a pioneering analytical study of the discontinuous phase (bubble) motion through a continuous viscous phase in a Hele-Shaw cell. The obtained exact solution did not consider the surface tension of the interface and viscosity of the discontinuous phase. The solution was not mathematically unique and the two-parameter (velocity and bubble area) families of solutions were obtained to specify the bubble shape. The solutions for a small bubble size (compared to the channel width) with non-zero viscosity in horizontal flow were also obtained. Tanveer[3-5] extended Taylor-Saffman's work by introducing the effect of surface tension on the shape and velocity of such bubbles and removed the degeneracy of their solution i.e., obtained a unique bubble speed for any surface tension and bubble area. However, the solution remained non-unique for the bubble shape and three branches with qualitatively different shapes were found. The first branch consisted of circles (high surface tension / low Capillary number, Ca=$U_d \mu_c / \sigma$) and elongated ellipses in the flow direction (low surface tension). The second branch showed an unexpected behavior consisting of circular bubbles (low surface tension), and shortened shape ellipses in the flow direction (high surface tension). The third branch were bubbles with negative curvature at their front stagnation point (some ranges of the surface tension). A wide range of propagation velocities higher than the velocity of the

conveying fluid was reported. Kolb and Cerro[6]theoretically analyzed the air bubble motion in a square channel filled with a stagnant liquid, and found that the liquid flow over the four corner regions exceed 95% of the total flow rate across the channel cross-section. Considering the fact that the sidewall film of the continuous phase shown in Fig. 1 is extremely thin, the no-flow assumption in the thin film would be reasonable.

The experimental studies are scant compared to the theoretical ones, and only a few experimental works on the motion of a discontinuous phase through a continuous phase in the Hele-Shaw cell have been reported. It also appears that the bubble motion has received far more attention than the flattened drop motion in the Hele–Shaw Cell.

Saffman and Taylor [7] describe the bubbles in their viscous fingering studies. The small bubbles were always circular and the larger ones were either pear-shaped with a rounded cap backward or ovoid with the sharper end pointing to the flow direction. They attributed the non-circularity shape effect to the thin film left between the bubble and the wall. No velocity data were reported. Eck and Siekmenn's [8] gravity driven bubble experi-ments in a Hele-Shaw cell show circular-shape bubbles at low Capillary numbers and shortened shapes in the direction of flow at higher Capillary numbers. The measured bubble velocities were smaller than the predicted bubble velocities and the dis-crepancy was more pronounced for smaller bubbles. They explained the discrepancy by including the capillary effects in the thin film left on the wall. Unlike Eck and Siekman, Maxworthy's [9] gravity driven bubble experiments showed elliptical bubbles with the longer dimension in the flow direction. He observed that large bubbles moved faster, while small circular shaped ones moved slower than expected.

Kops-Sill and Homsy's [1] experimental study of pressure driven single bubble flow in a horizontal Hele-Shaw cell showed a variety of steady bubble shapes and sizes with their characteristic velocities, over a range of Capillary numbers. They recorded six types of bubble shapes shown in Fig. 2. To explain why other authors did not observe some of these classes, they referred to the considerable differences between the Bond numbers (the gravity to interfacial force ratio, $\rho_c g R^2 / \sigma$, where ρ_c, g, R and σ are conveying phase density, gravitational acceleration, conduit radius and the surface tension, respectively). The flow will be interfacial tension dominated for Bond numbers less than 0.842 [10]. Accordingly, some bubble shapes require a laterally symmetric flow field. They did not explain why the bubbles have the specified shapes and also under what conditions the bubbles shape changes. Though most of these bubble shape classes can be obtained by Tanveer's simplified theory, the propagation velocities of bubbles cannot [3-5]. Their measured velocities were in the range of one fifth to twice that of the conveying fluid and thus very different from Tanveer's theoretical predictions. The discrepancy in the velocities was not explained. In a follow-up work, Saffman and Tanveer [11] suggested that the breakage of viscous fluid film between the bubble and the wall, and advancing-retreating interface contact angles could be the reasons. However, no clear explanation has yet been proposed for this problem. Different re-searchers' capillary numbers range, for various bubble shapes, do not match. So, it may be concluded that the shapes cannot be classified on the basis of this dimensionless number alone. Kopf-Sill and Homsy [1] confirmed Tanveer's theoretical multiple solutions to the bubble problem.

[12] Park et. al studied, systematically, the dependence of the bubble motion in a Hele-Shaw cell on the surfactant concentration. They tried to give an explanation to Kopf-

Sill and Homsy's perplexing observations by concluding that it may be due to the influence of surface-active contaminants. Maruvada and Park estimated the translational velocity of an elliptic bubble assuming that the conveying fluid wets the solid wall and that the bubble surface is rigid due to the surfactant influence.

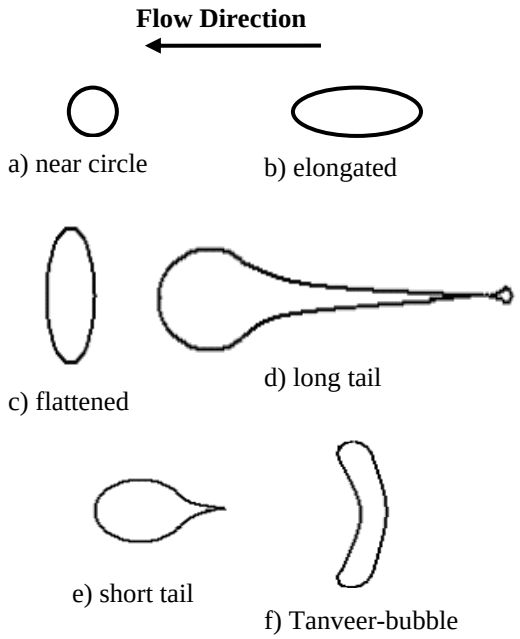

Figure 2. Various bubble shapes observed in Hele-Shaw cell (Kops-Sill and Homsy, 1988).

The objectives of the current work are to study the shapes of a single slug (large flattened drop) of a nonwetting phase moving with a viscous wetting phase through a Hele-Shaw cell and to evaluate the effect of flow conditions. The deformations of the elongated flattened drops were also evaluated. The results are useful for achieving a better understanding of oil-water two-phase flows in fractures and the relative permeability characteristics of the fractured media. The experimental approach was based on introducing a single elongated flattened drop into the conveying phase for various fluid systems. The conveying phase was oil for the oil-wet wall and water was used as the discontinuous phase. However, the results would be applicable to any discontinuous non-wetting phase in a conveying wetting phase in a Hele-Shaw Cell.

It is believed that the effect of the surfactant or contaminant should be considered in the capillary number; therefore no surfactants were used in these experiments.

2. Experimental Setup and Procedure

A schematic diagram of the test rig is shown in Fig. 3. The apparatus comprises a Hele-Shaw cell, water and oil supply lines, and a pressure transducer. The two flat plates were made of 15 cm thick Plexiglass and held together with bolts, creating a 0.034 cm gap between them by inserting metal shims between the plates. The fracture was 65 cm in length with two pressure taps 40 cm apart located along the centerline of the lower plate at distances of 10 and 15 cm from the entrance and exit, respectively. The pressure taps were connected to a differential pressure transducer to measure the pressure drop. The space between these two pressure taps was the test section. Three injection and production holes were drilled in the upper plate. The flattened drop velocity and size were measured in the test section of the cell, using a stop watch with a ruler attached to it. The test section is that part of the cell where the flow is uniform i.e., between the pressure tap holes. A light table, placed under the model, assisted in clear identification of the liquid-liquid interface. The water (or diluted glycerin) was injected through the middle port by an ISCO model 2350 HPLC pump. The oil was injected through the two lateral ports with a pair of ISCO syringe pumps (model 100DM). Both pumps were set for constant flow rate condition. The discharge was to the atmosphere through the outlet ports. The conveying phase volume flow rate was used to calculate its average velocity U_c.

The flattened drop was formed by injecting water (or diluted glycerin) at a constant flow rate into the flowing oil. Continuous

flattened drops of apparently equal size and spacing were formed. Obviously due to the limited model length, flow rates had to be set sufficiently small so that consecutive flattened drops did not significantly affect the flow field of a single flattened drop. The elongated flattened drop length was also kept small enough to have a steady-state condition at the test length section of the cell. The flattened drop volume was measured by weighing the fluid injected during the flattened drop formation using a two digit precision electronic balance as shown in Fig.3. The volume of each flattened drop may be used to determine its flattened surface area. As mentioned earlier, the drop velocity U_d was measured simply by measuring the time of travel over a distance marked on a ruler attached to the cell. An example of distance traveled by different size discontinuous phase versus time is shown in Fig.4.

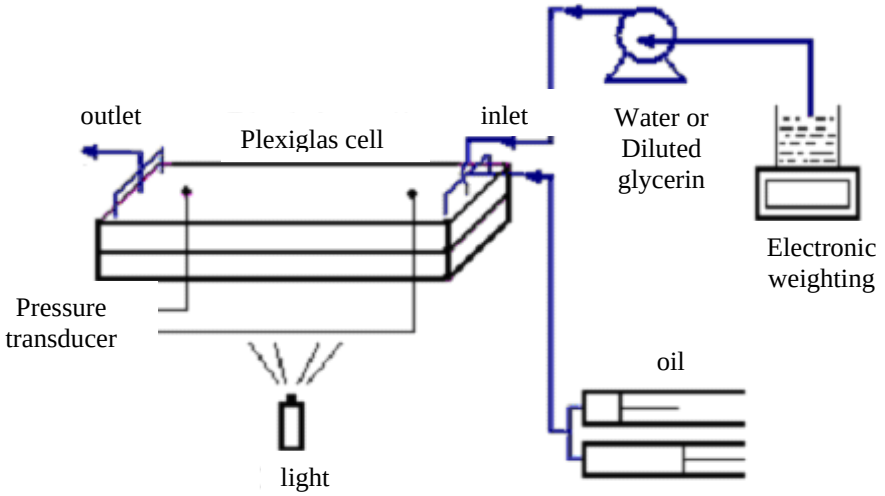

Figure 3. Schematic diagram of experimental set up.

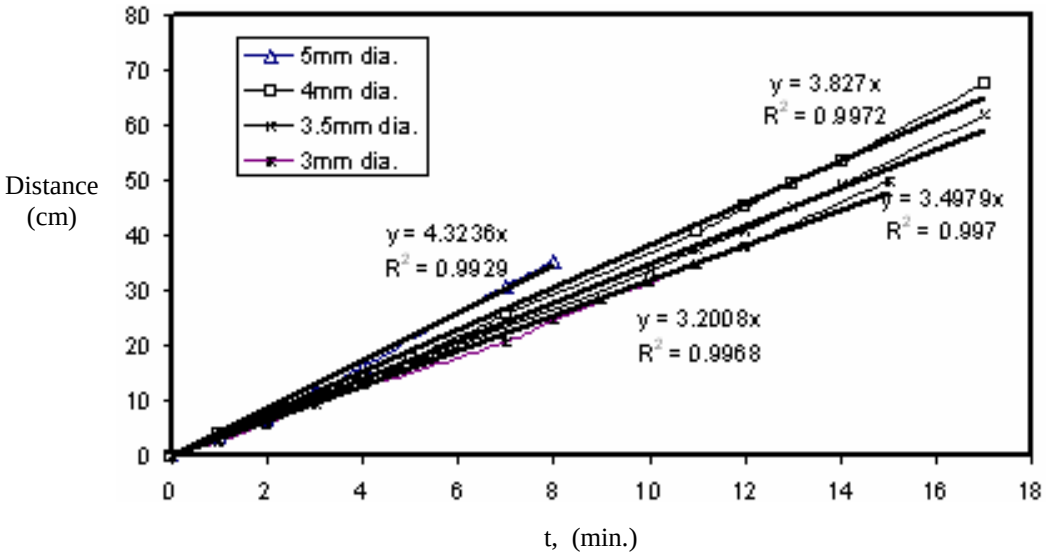

Figure 4. Distance traveled by the discontinuous phase versus time, to find U_d .

A digital camera was used to take pictures of the flattened drops. The images were stored for later analysis on a personal computer. "Image-Plus Pro" software was used with the captured images to characterize the shape of the fluid-fluid interface and geometrical properties of the flattened drop such as length, width and area.

The conveying oils were Vitrea22, Shell-flex810 and two more samples named Vitflex1 and Vitflex2 made by mixing Vitrea22, Shellflex810 and a small amount (0.1% by volume) of a heavy crude oil (from Elkpoint) to make it darker for better observations. The discontinuous phases were water and two different diluted glycerin solutions named gly1 and gly2. Viscosity and density of the samples were measured using a rotational viscometer (Thermo Haake Roto-Visco®1) and pycnometer at the experiment conditions. The interfacial tension was measured using a duNouy ring tensiometer (Fisher Surface Tensiomat, Model 21).

3. Results and discussions

Table 1 summarizes the seven different pairs of liquids used in the experiments for the range of conditions studied. The interfacial tensions are also listed in Table 1. The densities and viscosities of the samples are listed in Table 2. The effects of fluid properties and flow conditions on the flattened drop shape were recorded for the different Capillary number ranges and drop volumes shown in Table 1. The study of irregular flattened drop behavior in the capillary dominated regime requires a sufficiently low Capillary number (1.69×10^{-6}). Several single-phase flow tests, in which the steady-state pressure gradient was measured in the test section at different flow rates, were carried out. The results were consistent with the well-known cubic law for a single phase flow in fractures[13].

Table 1. Liquid-liquid systems used and the experiment conditions.

System #	Continuous phase	Discontinuous phase	Interfacial tension, mN/m	Capillary number range, $\times10^3$	Drop volume, $m^3\times10^3$
1	Vitrea22	Water	8	2.19 – 7.65	0.46 – 1.44
2	Vitflex1	Water	10	3.25 – 11.6	0.92 –1.41
3	Vitflex2	Water	13	3.42 – 20.1	0.17 – 1.34
4	Vitflex2	Gly2	17	2.49 – 21.3	0.28 – 0.97
5	Shellflex810	Water	19	8.01 – 30.4	0.29 – 1.31
6	Shellflex810	Gly1	35	1.03 – 15.1	0.61 – 1.55
7	Shellflex810	Gly2	23	2.49 – 21.3	0.11 – 0.68

Table 2. Physical properties of various fluids used at laboratory condition.

Fluid	Density, kg/m^3	Viscosity, mPa.s
Water	998	1
Gly1	1201	7
Gly2	1202	20
Vitrea22	858	45
Vitflex1	867	130
Vitflex2	880	335
Shellflex810	892	2245

The elongated flattened drop shapes

The flattened drop shape is the result of competition between the interfacial tension forces that tend to make the flattened drop circular and the viscous forces that tend to elongate it. Knowledge of the forces acting on the flattened drop by the surrounding fluid is of primary importance for the analysis of its shape and motion. The force exerted on the flattened drop by the conveying liquid is due to their relative motion. When a flattened drop moves faster than the conveying fluid (i.e. for positive slip velocity, $U' = U_d / U_c > 1$), the only driving force is the pressure difference across the elongated flattened drop, and the resistance against its motion (drag) is due to the viscosity of the conveying phase and the elongated flattened drop shape. The driving force in each run remains constant, while the drag force increases with the slip velocity. The terminal velocity will be the result of the balance between the driving force and the drag force. In general, elongated flattened drops tend to assume shapes that reduce the drag.

Fig. 5 shows several typical shapes of the stabilized elongated flattened drops observed for the range of Capillary numbers given in Table 1. The interfaces have been highlighted to clarify the elongated flattened drops.

The flattened drop shape shown in Fig. 5(a) is ovoid or elongated ovoid displaying lateral and longitudinal symmetries. It resembles the elongated bubbles reported by Kopf-Sill and Homsy [1] in their gas-liquid systems [Fig. 2(c)]. However, the elongated flattened drop shapes were ovoid with the sharp end pointing in the upstream direction in several other cases, [Fig. 5(b) and 5(c)]. These elongated flattened drops were similar to what Taylor and Saffman reported in their gas-liquid system. In spite of a similarity of the observed elongated flattened drop shapes with some elongated bubbles referred to in the literature, a significant difference in their velocity behavior was observed. The elongated flattened drop slip velocity was always positive ($U' = 2 - 4.7$), as opposed to those of Kopf-Sill and Homsy [1], which were negative ($U' = 0.2 - 0.55$). The elongated flattened drop shapes in this work were not exactly ellipse, however they were aligned with their longer axes in the direction of flow much like the elongated bubbles of Taylor and Saffman [7].

Typical profiles of elongated flattened drops can be assumed to comprise five zones similar to those of Liao [14] for the elongated bubble motion in capillary tubes. These are: leading zone, front transition (separating leading and flat zone), flat zone, rear transition zone and trailing zone. The shape differences may be described in terms of the leading-trailing radius of curvature and transition zone lengths. For example, the two transition zones in Fig. 5(a) have almost the same size and radius of curvature. However, in Fig. 5(b) the leading radius of curvature is much smaller than the trailing radius of curvature and the transition zone is asymmetric. For some elongated flattened drops the trailing zone was completely pointed so that its radius of curvature approached infinity. Fig. 5(c) is a case between those in Fig. 5(a) and 5(b). The results did indicate that the front transition zone radius of curvature and length is always less than that of the rear one, for all stabilized elongated flattened drops.

Helenbrook [15] believes that internal circulation of the elongated flattened drop cause a prolate shape. Because of the no-slip boundary condition at the interface, the lateral surfaces of the flattened drop move forward at a lower velocity than the interior. This sets up two circulation loops inside the flattened drop as shown in Fig. 6. The circulation pattern shown by streamlines in this figure leads to higher pressure at the leading and trailing edges. This, in turn, causes the flattened drop to become prolate. In other words, this shape is caused by the internal convection in the discontinuous phase.

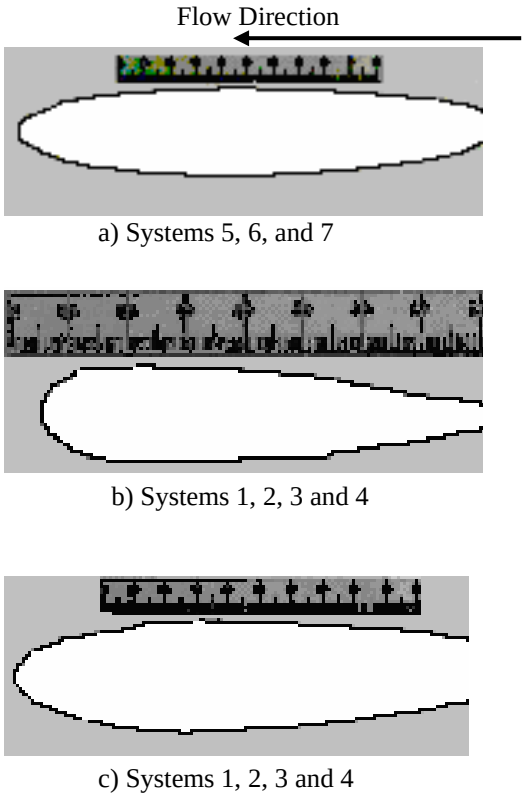

Figure 5. Typical shapes of stabilized elongated flattened drops.

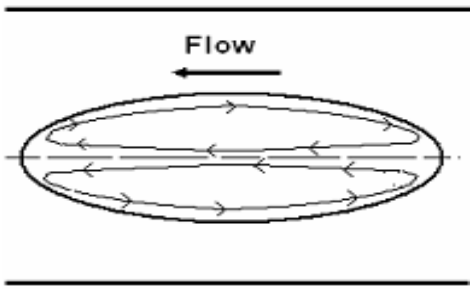

Figure 6. Internal circulation (Hill Vortex) in an elongated bubble.

The experimental observations showed that decreasing the capillary numbers down to values that often occur in flow through natural fractures in petroleum reservoirs cause the drops to assume an irregular unstable-shape. The slip velocity of the flattened drop has an important role in establishing the flattened drop shape. At very low slip velocity the form drag force vanishes and therefore the tendency of a flattened drop to assume an aerodynamic shape ceases to exist. Under these quasi-static flow condi-tions (sufficiently low flow rates), the phase structure in the cell is strongly affected by the interfacial forces. However, when the drop is large, the interfacial force that tends to make the drop circular is also weak and the drop shape is

controlled by variations in the local surface properties such as roughness and/or wettability.

Fig. 7 illustrates two elongated flattened drops under such conditions; Fig. 7(a) for lower and Fig. 7(b) for higher capillary number. As the Capillary number increases, the effect of surface properties on the interface shape decreases.

It was observed that the interface instability always starts from the rear part (upstream) of the flattened drop. Further decrease of the Capillary number advances the irregularity toward the middle and finally to the front of the elongated flattened drop. At low Capillary numbers (capillarity dominated region) the flattened drop shape was completely irregular and unstable (Fig. 8). Unlike the stabilized elongated flattened drops, the velocity of the irregular one was much smaller than U_c (negative slip velocity) for very low Capillary numbers. Figs 8(b) and 8(c) show the flattened drop shapes 20 and 50 minutes after decreasing U_c from 0.129 to 0.016 167 cm/s, respectively. Due to the instability of the flattened drop shape, accurate measurement of the drop velocity was difficult. The flattened drop shape 165 min after further decrease of U_c is shown in Fig 8(d). Some experiments showed the detachment of small segments from the rear end of the flattened drop.

A different type of instability appeared when the continuous phase velocity was increased by a large margin beyond the stabilized elongated flattened drop velocity case. The longer the original elongated flattened drop, the higher the instability tendency. The flat zone interface disappeared. Fig. 9 shows an example of such a wavy interface behavior after increasing U_c by a factor of two in system 6. Many experimental results showed that, for the same U_c, the instability depends on the elongated flattened drop length, i.e. after a certain length the shape becomes unstable.

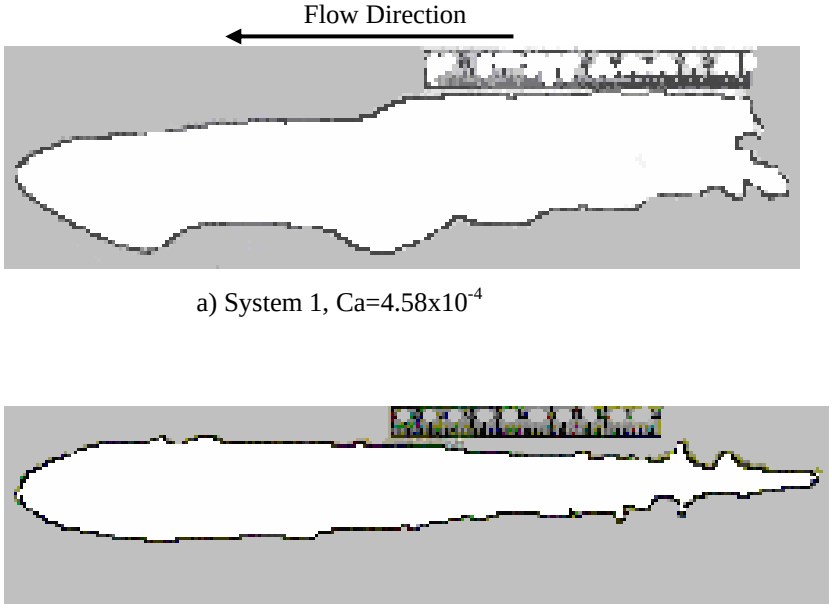

a) System 1, Ca=4.58x10^{-4}

b) System 2, Ca=1.66x10^{-3}

Figure 7. Irregularity in the elongated flattened drop shape at low Capillary numbers.

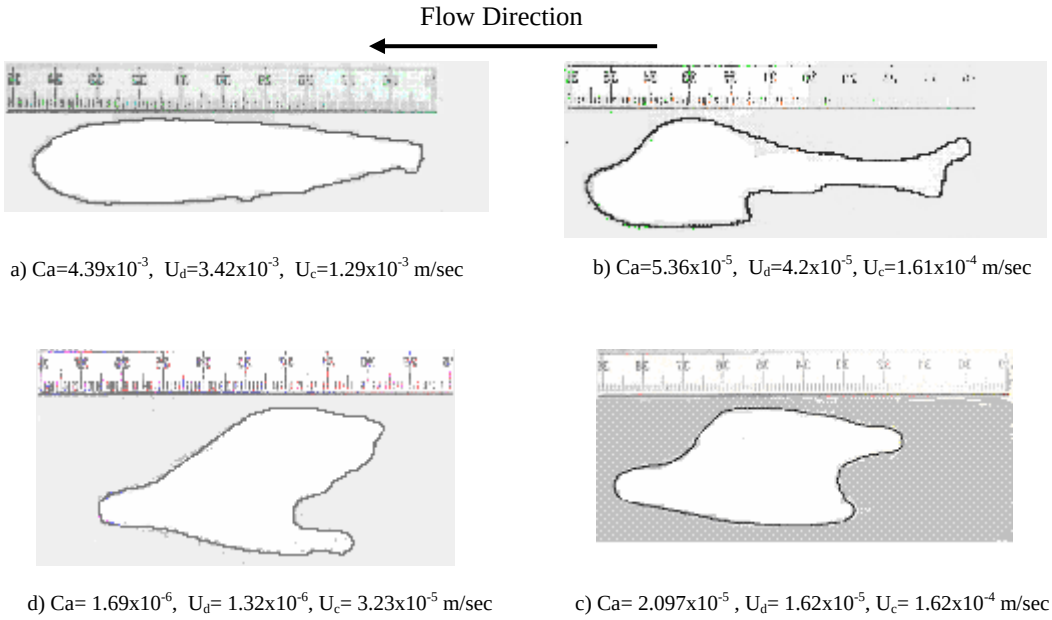

Figure 8. Variation of the unstable-interface shape caused by decreasing Capillary number for system 1.

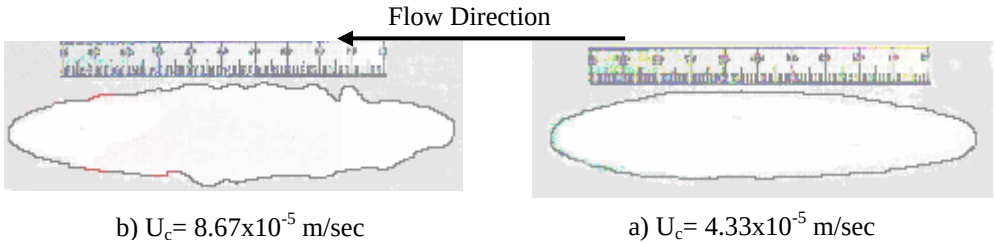

Figure 9. Interface instability caused by increasing the surrounding liquid velocity for system 6.

Occasionally there was a collision between a stabilized elongated flattened drop and a small circular flattened drop (less than 4 mm in diameter), i.e. a faster moving large elongated flattened drop caught a slower moving small circular flattened drop. There were two dramatically different interactions between flattened drop shapes for different systems and dynamic conditions. Sometimes the elongated flattened drop and small circular one simply coalesced, while in other cases the small flattened drop acted like a rigid particle and caused the elongated flattened drop to bifurcate. Smaller size circular flattened drops or higher surrounding liquid velocities show a higher tendency to bifurcate the elongated flattened drops. However, the bifurcation of elongated flattened drops by small circular flattened drops never happened for the velocity ranges used in systems 1-4. These observations are quite different from those of Maxworthy's [9] gravity driven bubble experiments. His experiments showed that small bubble and very large elongated bubble collision would induce a symmetric wavelike instability on the elongated bubble interface. It is interesting to note that the reported pictures of instability in his paper are similar to the one shown in Fig 9(b).

Fig. 10 illustrates the effect of U_c on the shape of two equal volume flattened drops of system 1. The L_d and W_{dm} in Fig. 10 are the flattened drops length and maximum width, respectively. Wavelike instability appeared with continued increase, in the velocity U_c, as mentioned earlier.

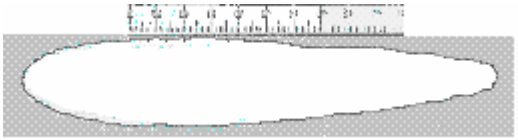

a) U_c= 6.62x10^{-4} /sec, L_d= 0.17 m, W_{dm}= 0.031

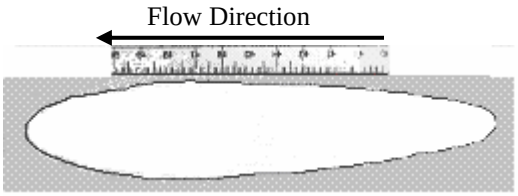

b) U_c= 1.63x10^{-3} m/sec, L_d= 0.16 m, W_{dm}= 0.035

Figure 10. Effect of increasing Uc on prolating of an elongated flattened drop in System 1.

Quantitative prediction of the elongated flattened drop deformation is a difficult task. The problem's complexity requires numerical simulation. To the authors' knowledge, neither an analytical relation nor any empirical correlation has been reported in the literature for this phenomenon in Hele-Shaw cells.

Understanding how the elongated flattened drop shape changes as a function of flow conditions is of interest. For this purpose a single parameter, namely the aspect ratio, was selected to describe the deformation. The aspect ratio A_R is defined as the ratio of the centerline length of the flattened drop to its maximum width. It is expected that fluid properties as well as the cell geometry would affect the results. Another important parameter, as mentioned before, is the discontinuous phase velocity. Furthermore, observations did indicate that the lager volume flattened drops are more elongated. Therefore, the flattened drop volume is also an important parameter in determining the aspect ratio. Fig. 11 presents experimental results showing the effect of flattened drop volume at constant Capillary number.

The parameters that were considered relevant are: fluid viscosities, interfacial tensions, cell width, gap size, elongated flattened drop volume and velocity. Since the magnitude of the Bond number in the experiments was very small (much less than 0.842), the gravity force was ignored. Also, since the velocities involved were very small, inertial effects were considered unimportant. Dimensional analysis was used to develop dimensionless numbers that affect the aspect ratio. Four dimensionless numbers, including b/W, $U_d\mu_d/\sigma$, $U_s\mu_c/\sigma$ and b^2W/V were obtained, where b, W, U_s, V and μ_c are cell gap size, cell width, slip velocity, elongated flattened drop volume, and continuous phase viscosity, respectively.

Experimental results were used to evaluate the influence of these dimensionless numbers. The first one, (b/W), was kept constant. Since $b \,\&\, W_{dm} << W$, the effect of b/W is not likely to be significant. The results showed that the second dimensionless number also did not have a significant effect. A correlation was developed between A_R, Ca, and S_N based upon the experimental data as:

$$A_R = 0.8\ S_N{}^{0.28}\ Ca^{0.043} \qquad (1)$$

Where,

$$S_N = \frac{b^2 W}{V}, \qquad Ca = \frac{U_s \mu_c}{\sigma} \qquad (2)$$

S_N is the dimensionless size number and Ca is the capillary number based on the slip velocity of the drop. It was found that in the

definition of the Capillary number, U_d is more appropriate than U_c or U_d, since it is the slip velocity that controls the deformation.

Fig. 12 shows a comparison of the aspect ratio predicted by Eq. (1) versus the experimental results. In most cases, Eq. (1) predicts the aspect ratio of the elongated flattened drops to within a 10% error.

No dependency of the aspect ratio to the viscosity of the discontinuous phase was observed. The size number S_N appears to be the most important parameter. Netto et al. [16] pointed out the dependency of elongated bubble shape to its length for the motion of long isolated air bubbles in water flowing through pipes (not in Hele-Shaw cell).

Eq.(1) also shows that the aspect ratio is a weak function of the capillary number.

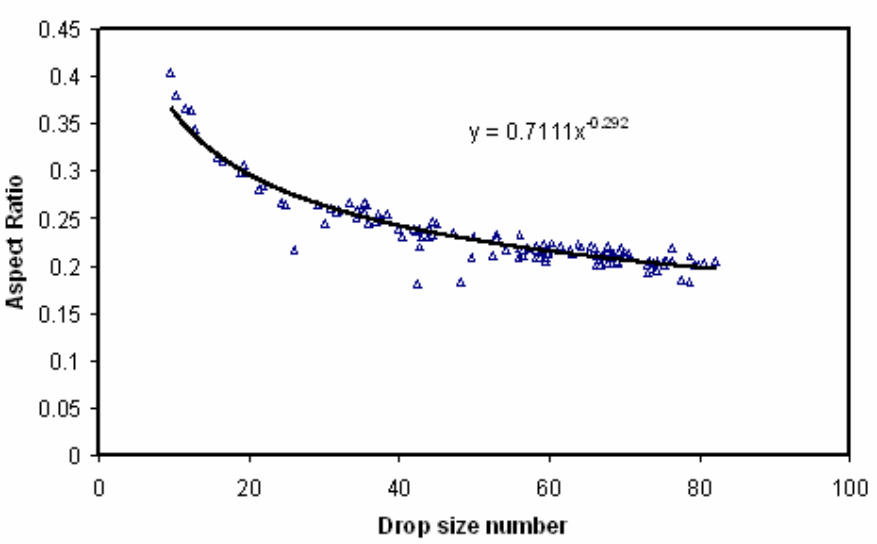

Figure 11. Effect of the flattened drop size number on the aspect ratio.

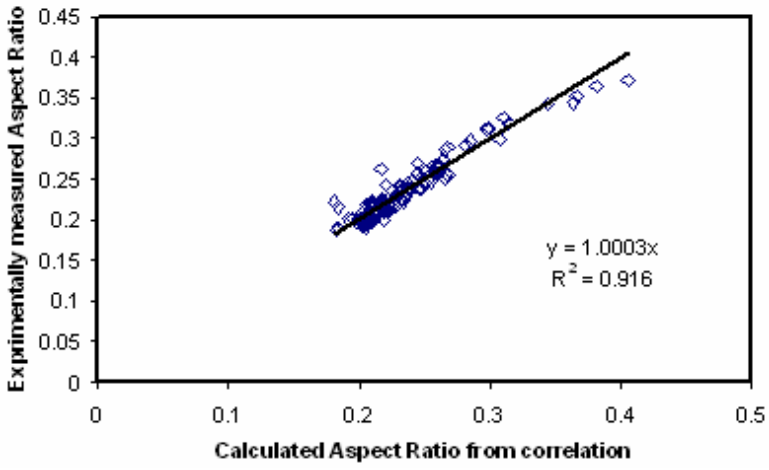

Figure 12. Measured elongated flattened drop aspect ratio versus predicted values based on Equation 1.

4. Conclusions

A number of experiments have been performed to study the shapes of elongated flattened drops of a non-wetting phase in a horizontal fracture. Three different shapes of stable-elongated flattened drops were observed and these results were compared with the results reported in the literature for gas-liquid systems. In spite of the similarity of the observed elongated flattened drop shapes with those reported in the literature, a significant difference in the velocity behavior was observed. Using the aspect ratio as a measure of the elongated flattened drop shape, a correlation was developed to predict the shape of stable-elongated flattened drops as a function of the flow capillary number, as well as the drop size number. The correlation represents the measured data points within ±10% for almost all ob-servations.

The results also showed that continuously increasing the conveying phase velocity increases the slip velocity, and eventually a wavy instability develops at the interface of the elongated flattened drop.

Decreasing the capillary number beyond a certain value also introduced deformations at the interface. This irregularity on the interface always started from the rear part of the flattened drop. Decreasing the capillary number continuously caused the irregularity to advance toward the middle part and finally, to the nose of the flattened drop. Such irregular flattened drops had velocities much smaller than the velocity of the continuous phase. These cases may occur more often in real natural fractures.

Nomenclature

A_R	Ratio of the centerline length of the flattened drop to its maximum width
b	Fracture opening (aperture), cm
Ca	Capillary number defined as $\mu_c U_d / \sigma$
g	Gravitational acceleration, m/s^2
L_d	Length of elongated flattened drop, mm
r	Radius of the circular flattened drop, mm
R	Radius of the conduit, m
S_N	Size number defined as b^2W/V
U_c	Conveying phase velocity, cm/s
U_d	Flattened drop phase velocity, cm/s
U_s	Slip velocity of the drop, cm/s
U'	Velocity ratio (flattened drop to the surrounding liquid), dimensionless
V	Volume of the elongated flattened drop, m^3
W	Channel width, cm
W_d	Flattened drop phase width, mm
W_{dm}	Maximum flattened drop phase width, mm
μ_c	Flattened drop phase viscosity, Pa.s
μ_d	Conveying phase viscosity, Pa.s
ρ_c	Flattened drop phase density, kg/m^3
σ	Interfacial tension, mN/m

Acknowledgements

The authors wish to express their gratitude to the Petroleum University of Technology, Islamic Azad University of Ahwaz and the Department of Chemical & Petroleum Engineering of the University of Calgary for their helpful collaboration.

References

1. Kopf-Sill, A.R. and Homsy, G.M. *Bubble motion in a Hele-Shaw cell.* Physics of Fluids, 1988. 31(1): p. 18-26.
2. Taylor, G.I. and Saffman, P.G. *A note on the motion of bubbles in a Hele-Shaw cell and porous medium.* J. Mech. Appl. Math., 1959. 12: p. 265-279.
3. Tanveer, S., *The effect of thin film variations and transverse curvature on the shape of fingers in a Hele-Shaw cell.* Physics of Fluids, 1987. 30: p. 2617-2623.
4. Tanveer, S., *New solutions for steady bubbles in a Hele-Shaw cell.* Physics of Fluids, 1987. 30(3): p. 651-658.

5. Tanveer, S., *The effect of surface tension on the shape of a Hele-Shaw cell bubble.* Physics of Fluids, 1986. 29(11): p. 3537-3548.
6. Kolb, W.B. and Cerro, R.L. *Film Flow in the Space between a Circular Bubble and a Square Tube.* Journal of Colloid and Interface Science, 1993. 159(2): p. 302-311.
7. Saffman, P.G. and Taylor, G.I. *The penetration of a fluid into a porous medium or Hele-Shaw cell containing a more viscous liquid*. in *Pro. R. Soc. London*. 1958.
8. Eck, W. and Siekmann, J. *Bubble motion in a Hele-Shaw cell, a possibility to study 2-phase flows under reduced gravity.* Ingenieur-Archiv, 1978. 47: p. 153-168.
9. Maxworthy, T., *Bubble formation, motion and interaction in a Hele-Shaw cell.* J. Fluid Mech., 1986. 173: p. 95-114.
10. Bretherton, F.B., *The motion of long bubbles in tubes.* J. Fluid Mech., 1961. 10: p. 166-188.
11. Saffman, P.F. and Tanveer, S. *Prediction of bubble velocity in a Hele-Shaw cell: Thin film and contact angle effects.* Physics of Fluids A, 1989. 1(2): p. 219-223.
12. Park, C.-W., Maruvada, S.R.K. and Yoon, D.Y. *The influence of surfactant on the bubble motion in Hele–Shaw cells.* Physics of Fluids, 1994. 6(10): p. 3267-3275.
13. Snow, D., *A parallel plate model of fractured permeable media*. 1965, University of California: Berkeley, CA.
14. Liao, Q. and Zhao, T.S. *Modeling of Taylor bubble rising in a vertical mini noncircular channel filled with a stagnant liquid.* International Journal of Multiphase Flow, 2003. 29(3): p. 411-434.
15. Helenbrook, B.T. and Edwards, C.F. *Quasi-steady deformation and drag of uncontaminated liquid drops.* International Journal of Multiphase Flow, 2002. 28(10): p. 1631-1657.
16. Fagundes Netto, J.R., Fabre, J. and Peresson, L. *Shape of long bubbles in horizontal slug flow.* International Journal of Multiphase Flow, 1999. 25(6-7): p. 1129-1160.